Characterization of the Ge/Bi$_2$O$_3$ Interfaces

Seham Reef Alharbi[a], Atef Fayez Qasrawi[b,c] *

[a]Department of Physics, Faculty of Science, University of Jeddah, Jeddah, Saudi Arabia
[b]Department of Physics, Arab American University, Jenin, Palestine
[c]Group of physics, Faculty of Engineering, Atilim University, 06836 Ankara, Turkey

In this article, the properties of the Ge/Bi$_2$O$_3$ interfaces as microwave cavities are reported and discussed. The interface is composed of monoclinic Bi$_2$O$_3$ films grown onto polycrystalline cubic Ge substrate. It is observed that consistent with the theoretical design of the energy band diagram, the experimental current-voltage characteristics of the Yb/Ge/Bi$_2$O$_3$/C hybrid device structure exhibits electronic switching property. In addition, the capacitance, resistance and microwave cutoff frequency spectral analysis in the frequency domain of 0.01-1.50 GHz revealed a frequency dependent tunability of the device. Moreover, while the Yb/Bi$_2$O$_3$/C interface displays negative capacitance effect, the Yb/Ge/Bi$_2$O$_3$/C interfaces are also found to have the ability of altering the resistance up to three orders of magnitude. Such property allowed reaching a cut off frequency up to 116 GHz. The electronic features of the device indicated that the Ge/Bi$_2$O$_3$ interfaces are attractive for production of negative capacitance field effect transistors and band pass/reject filters.

Keywords: *Ge/Bi$_2$O$_3$, heterojunction, X-ray, electronic switch, microwave cavity.*

1. Introduction

In Recent years, developing multifunctional devices has attracted the attention of research society as such property lowers the cost and size of electronic systems. As an example of such devices, an integrated multifunctional flexible device which is made of a supercapacitor and electrochromic material is reported to behave as a highly stable supercapacitor, and also as solar cells. The system is observed to be able to simultaneously harvest, store, and use the renewable energy efficiently [1]. As another example of multifunctional operations, heterojunctions made of n-type silicone-carbon nanotubes are observed to be able to behave as a pressure sensor and as a solar cell [2].

One of the promising materials that are beneficial for multifunctional operations is the Bi$_2$O$_3$ in thin film form. Analyses of the current-voltage characteristics of the devices (MgF$_2$/γ-MnO$_2$/α-Bi$_2$O$_3$/a-Si solar cell) that get use from Bi$_2$O$_3$ are found to reveal a solar energy efficiency of 3.28 % [3]. This material is also used to produce multifunctional devices that can exhibit ferroelectric, ferromagnetic and magnetodielectric coupling characteristics at the same time [4]. In addition, the sensitization of the TiO$_2$ with Bi$_2$O$_3$ nanoparticles is reported to play remarkable improvements in the visible light absorbability and enhanced the solar energy efficiency [5].

Unfortunately, optimizing high efficiency electronic device from the Bi$_2$O$_3$ is rarely observed. One of the materials that is known for its performance in electronic technology is the germanium. An ultra-thin layer of hydrogenated amorphous germanium is reported to have the potential of replacement of standard micrometer-thick microcrystalline silicon absorbers in silicon thin-film solar cell technology [6-8]. The strong absorption of the Germanium ultrathin type cells revealed an efficiency of 11%. Ge films deposited onto GaAs also exhibited a high power conversion efficiency of 6.72% [9]. On the other hand, the SiGe solar cell in a GaAsP-SiGe dual junction which are prepared onto Si substrate is reported to be able to achieve an efficiency of 9.1% [10]. Beside these applications of Ge, the germanium in thin film forms can also be used for data transfer with rates that can reach 40 Gb/s [11]. This remarkable record makes it of favorite for communications technology. In addition, the Ge as active material is reported to exhibit plasmonic photodetector characteristics brightened by the high speed feature at nanoscale levels [12,13].

Bismuth oxide compound which is known for its additional wide range of applications as devices in optoelectronics [14], as catalyst material [15], as photoanodes [16] and as degrading materials [17] are prepared by various methods. As for example, the (δ-Bi$_2$O$_3$)$_{0.93}$(TiO$_2$)$_{0.07}$ nanocomposite thin films which were synthesized by pulsed laser technique onto glass substrates are found to be good optical material that can be used in fabricating optoelectronic devices [6]. In addition, Bi$_2$O$_3$ thin films which are prepared by the citrate-nitrate gel combustion method are reported to be good candidates as photoanodes [16]. In addition, Bi$_2$O$_3$ films which are prepared by the hydrothermal method are suitable for the degradation of methyl orange [17]. The method of preparation play important role on the polymorphic phase of Bi$_2$O$_3$. Five polymorphic phase of Bi$_2$O$_3$ called α, β, γ, δ and ω-Bi$_2$O$_3$ are reported [17]. While the low-temperature α-phase and high-temperature

*e-mail: atef.qasrawi@aaup.edu

δ-phase are stable, the other phases are high-temperature metastable phases. Most of these phases are producible by the hydrothermal and thermal evaporation [13] methods. The thermal evaporation which allow temperature controlled nucleation process is favorite where a single particular phase is requires because there exist a possibility of controlling both of the source and substrate temperatures [13].

The smart features of the germanium and Bi_2O_3 as thin film materials that can be employed in electronic technology motivated us to bring these two materials together. The purpose of this combination is to form a multifunctional device that can handle more than one duty at the same time. For this reason, here in this project we will form a Ge/Bi_2O_3 interface and study the interface basic characteristics as well as application directed features. The Ge/Bi_2O_3 heterojunctions which are deposited onto Yb substrates will be subjected to structural, morphological and resistance and capacitance spectral analyses. In addition, the current-voltage characteristics tests will be carried out to reveal further electrical properties.

2. Experimental Details

Yb, Ge and Bi_2O_3 thin films are prepared by the thermal evaporation technique using VCM-600 physical vapor deposition system. The Ge was grown onto Yb and glass substrates kept at 300 ºC under vacuum pressure of 10^{-5} mbar. The grown glass/Ge and Yb/Ge substrates are used to deposit Bi_2O_3 thin films. Both of the Ge and Bi_2O_3 are of thickness of 500 nm. The films thicknesses are monitored with the help of an in situ INFICON STM-2 thickness monitor. The X-ray analysis of the grown films are carried out by Miniflex 600 diffractometer. The scanning electron microscopy imaging is actualized with COXEM 200 SEM system. The carbon (99.99%) paste was used to make point contacts to the samples. Three channels named Yb/Ge/C, Yb/Bi_2O_3/C and Yb/Ge/Bi_2O_3/C were fabricated on the same device. The current-voltage characteristics of the channels are recorded with the help of Keithley current-voltage characteristics system. The resistance and capacitance spectra are recoded with the help of (10-1800 MHz) Agilent impedance analyzer.

3. Results and Discussion

Based on our previous studies which concerned novel characteristics of the Yb/Bi_2O_3/Au [13] Schottky barriers, here in this work we design multifunctional thin film transistors made of p-Ge, p-Bi_2O_3 and Ge/Bi_2O_3 channels deposited onto Yb substrate. In accordance with literature data, the Ge and Bi_2O_3, exhibit electron affinities of values of 4.13 [18] and 4.94 eV, respectively. The respective work functions of these two materials are 4.80 and 6.33 eV [13]. Since the Yb metal whose work function is 2.51 eV, it forms Schottky battier with both materials. As the proposed energy band diagram of the device which is displayed in Fig. 1 (a) shows, the Ge/

Bi_2O_3 heterojunction device is a broken gap heterojunction (type -III) in which the conduction band of Bi_2O_3 is lower than the valence band of Ge. For this type of heterojunctions an overlapping between the conduction band of Bi_2O_3 and the valence band of Ge can exist [18]. The top contact of the interfaces are made of carbon ($q\phi_c$ =5.10 eV) which also forms Schottky arms. Thus, the proposed hybrid device is composed of back to back Schottky diodes at sides of p-p heterojunction. The importance of this heterojunction device lays in the ability of the electrons which leave the valence band of Bi_2O_3 to arrive at the valence band of Ge or conduction band of Bi_2O_3. Such property is reported to make the heterojunction exhibits high mobility and high concentration field effect transistor characteristics [19]. The biasing of oxide layers is reported to allow carrier transfer without doping. This property reduces the high scattering and dominates the IC industries.

Fig. 1 (b) shows the optical image for the real device. The first channel (assigned as 1 in Fig. 1 (b)) is defined between Yb base and Ge/C interface. The second is Yb/Bi_2O_3/C and the third is Yb/Ge/Bi_2O_3/C (assigned as 2 and 3, respectively in Fig. 1 (b)). The homogeneity of the fabricated device is shown in Fig. 1 (c). The figure shows a representative enlargement of 24,000 times for the interface region between Bi_2O_3 and Ge/Bi_2O_3. As the figure displays, well oriented tiny grains are homogenously distributed over all the region. The average grain size of the grains is ~20 nm.

In order to investigate the nature of formation of the heterojunction, the X-ray diffraction technique is used. The resulting X-ray diffraction patterns are shown in Fig. 2. The figure compares the crystalline natures of each channel. It is clear from the sharp patterns that all the layers are of polycrystalline nature. The analysis of the observed diffraction peaks in accordance with the "TREOR 92" and "Crystdiff" software packages have shown that the Yb film exhibits face centered cubic structure with lattice parameter of value of a = 5.370 Å. Germanium thin films which are prepared at substrate temperature (T_s) of 300 ºC also exhibited polycrystalline cubic structure of lattice parameter a = 5.471 Å. The lattice mismatches between the base (Yb) and the Ge (first channel) is $\Delta\% = \frac{|a_{Ge} - a_{Yb}|}{a_{Ge}} = 1.81\%$ [18]. On the other hand, the indexing of the observed X-ray diffraction peaks for the Bi_2O_3 thin films which are deposited onto Yb substrate indicated that the preferred structure is mostly monoclinic. The unit cell lattice parameters for this phase of structure are a = 5.848, b = 8.166, c = 7.510 Å and β=113º. One minor peak of intensity of 25.5% with respect to maximum peak intensity (100%) is assigned to the tetragonal phase of Bi_2O_3. The lattice parameters which are reported here for the monoclinic unit cell are in good agreement with literature data [20]. Bi_2O_3 is known to exist in more than one polymorphic phases. The most famous phases are monoclinic α- and tetragonal β- phases. While the structure of the α- phase is formed from equidistant layers parallel to the yz-plane and every second
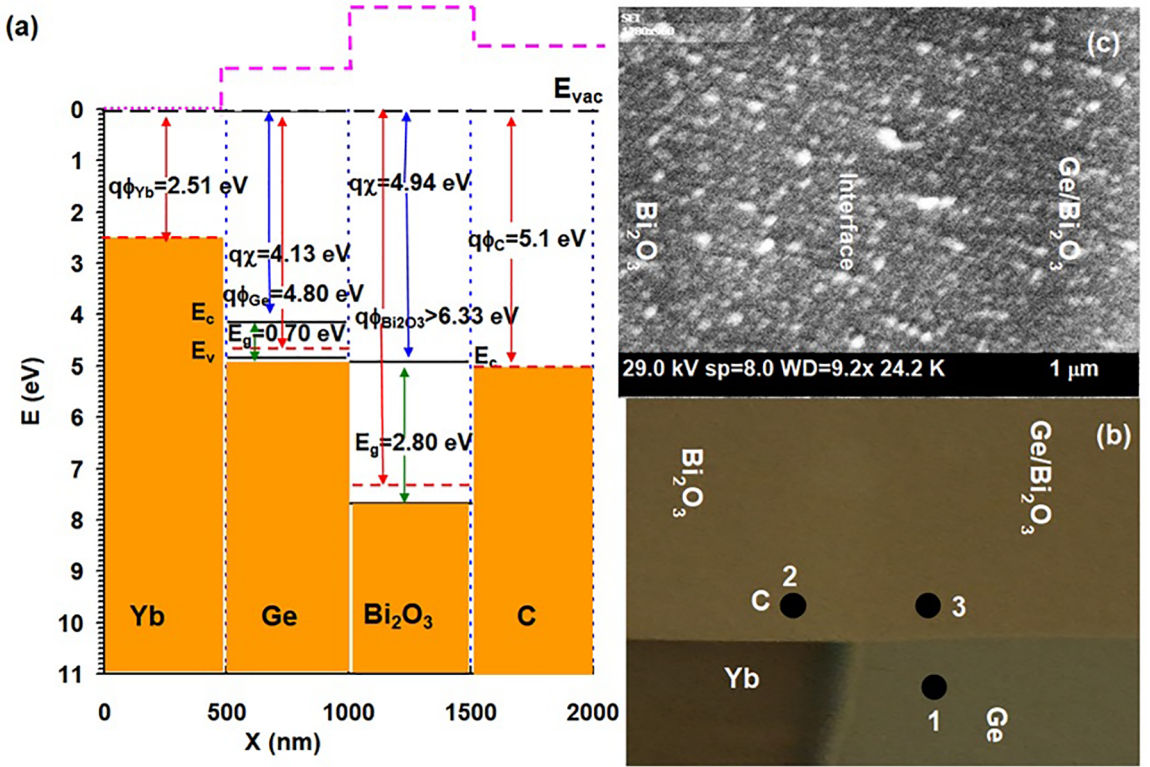
Figure 1. (a) The energy band diagram, (b) the optical image and (c) the scanning electron microscope image for the Ge/Bi$_2$O$_3$ device.
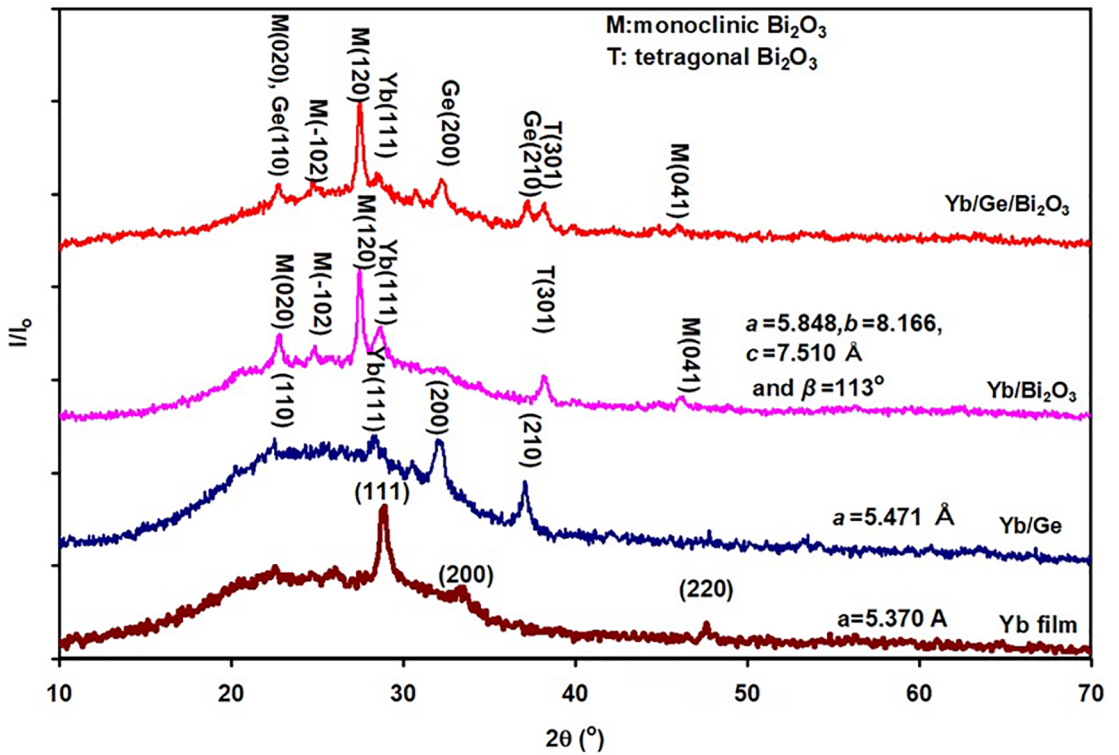

Figure 2. The X-ray diffraction patterns for the Ge/Bi$_2$O$_3$ interface deposited onto glass and Yb substrates

layer consists of bismuth atoms, the β- phase has the Bi atoms arranged in face centered cubic subshells with lattice parameter *a*=5.50 Å. In β- phase the coordination about the Bi atom is four folds and the coordination polyhedron is described by a distorted trigonal bipyramid in which one of the basal corners is occupied by the electron pair [20]. In accordance with the literature data, the monoclinic α- phase exhibits transition to the face centered cubic δ- phase by heating the compound at 730 ºC [21]. It is mentioned that owing to the large thermal hysteresis during the natural cooling cycle, δ- phase transform to tetragonal β- phase (usually stabilize at 650 ºC) and to body centered cubic (bcc) γ- phase. The bcc phases result from controlled cooling of δ phase. Both of the β- and δ phases convert to the monoclinic phase in the temperature range of 500-650 ºC [21]. In our previous investigation [13] we have reported that the Bi_2O_3 thin films which are deposited onto Yb substrate exhibit body centered cubic γ- phase. In order to discover the reason beyond the changes in the structure type in spite of using the same Yb substrate. We have run different growth cycles and we observed that, the films which are grown at an evaporation rate of 10-15 Å/*s* usually reveal the γ-phase. Films which are prepared at high evaporation rates of ~40 Å/*s* stabilize as α-phase.

Consistent with what we observed from the X-ray diffraction patterns of the Yb/Bi_2O_3, the Yb/Ge/Bi_2O_3 also revealed the same type of structure. The Yb/Ge/Bi_2O_3 heterojunction exhibits the same values of lattice parameters. No significant shift in the main peak position was observed. The major peak of the Yb/Bi_2O_3 which is oriented in the (120) direction are more intensive than that of Yb/Ge/Bi_2O_3 interface. The lattice mismatches between the Ge films and Bi_2O_3 along the *a, b* and *c*-axes are 6.4%, 33.0% and 27.2%, respectively. These values are sufficiently high to nominate the heterojunction device for optoelectronic technology applications. Large lattice constant mismatched heterojunctions mostly exhibit Misfit dislocations that can produce dangling and wrong bonds at the Ge/Bi_2O_3 interface. The dangling bonds may create deep trap states which enhance the recombination of the generated holes and electrons at the heterojunction interface. Such type of recombination is reported to be detrimental to open-circuit voltages than recombination in the absorber bulk for wide-bandgap solar cells [22].

As practical application to the proposed Yb/Ge/Bi_2O_3 interface, the current (*I*)-voltage (*V*) characteristics for the three channels is recorded and presented in Fig. 3 (a). The figure displays interesting features of the *I - V* curves. The curve displays typical Schottky device characteristics. While there is no difference between the three channels during the reverse biasing process, the forward biased Schottky channels displayed switching property. In other words, the forward current exhibits a jump from low to high current values at critical voltage shown by dashed circular shapes in the figure. Particularly, the Yb/Ge/C, Yb/Bi_2O_3/C and Yb/Ge/Bi_2O_3/C channels switch from low to high current at biasing

voltage of 0.14, 0.28 and 0.41 V, respectively. We believe that the differences in the switching voltage value are due to the lattice mismatches between the respective interfaces as we discussed in the X-ray analysis part. The less the lattice mismatch the lower the switching voltage. On the same context, the jump from low to high current values at particular voltage can be assigned to the electric field dependence of energy barrier height. Analysis of the forward *I-V* curves in accordance with the Schottky-Richardson theory [18] using the equation, $I = AA*T^2 \exp\left(-\frac{q\phi}{kT}\right)\left(\exp\left(\frac{qV-IR_s}{nkT}\right)-1\right)$ reveals ideality factor (*n*) values of 2.41, 2.82 and 3.06 for the first, second and third channel, respectively. These values correspond to a series resistance of average value of ~40 *kΩ* and barrier height (*φ*) values of 0.81, 0.98 and 0.94 eV, respectively. The Richardson constants values ($A* = 120m*$) is calculated from the effective masses of the holes in Ge ($m* = 0.285\ m_o$ [20]), Bi_2O_3 ($m* = 1.34\ m_o$ [23]),) and Ge/Bi_2O_3 ($m* = (m*_{Ge}^{-1} + m*_{Bi2O3}^{-1})^{-1} = 0.235 m_o$) at room temperature. The barrier height values lower to 0.77 eV as the applied voltage exceeds 0.5 V. All the channels exhibit the same value of current above 0.50 V. The increase in the barrier height value upon interfacing of Ge with Bi_2O_3 is attributed to the large lattice mismatch between the two layers. On the other hand, the deviation of the ideality factor from unity may be ascribed to the generation and recombination dynamics in the depletion regions, the high injection effect, the tunneling of the charge carriers between the valence band of Ge and conduction band of Bi_2O_3 (Fig. 1 (a)) and the surface effects [18].

Another practical application of the three channel device is demonstrated by the resistance and capacitance spectral analysis in the frequency domain of 0.01-1.50 GHz. The imposed Ac signal between the terminals of the device propagates while the device is at 0.10 V biasing voltage, The resistance spectra are displayed Fig. 3 (b). It is clear from the figure that the resistance spectra are highly sensitive to the signal frequency. It follows a logarithmic type of decay. It decreases by three orders of magnitude when signal propagates between the terminals of Yb/Ge/C (Channel 1) and terminals of Yb/Ge/Bi_2O_3/C (channel 3). The resistance responsivity to the signal frequency is very slow when it is imposed through Yb/Bi_2O_3/C (channel 2) terminal contacts. The difference in the resistances values as the terminal is changed provide an excellent tunability of the device when used as microwave cavity. On the other hand the capacitance spectra which are shown in Fig. 4 (a) and its inset indicate a relatively slower logarithmic decay compared to the resistance spectra. The capacitance spectra of the first and third channel decrease from 6.6 to 2.2 pF and from 4.7 to 3.9 pF as the frequency increases from 0.01-1.5 GHz, respectively. The capacitance spectra of the second channel which is shown in the inset of Fig. 4 (a) exhibits very different trend of variation presented by very fast decay followed by negative capacitance effect. Namely, the
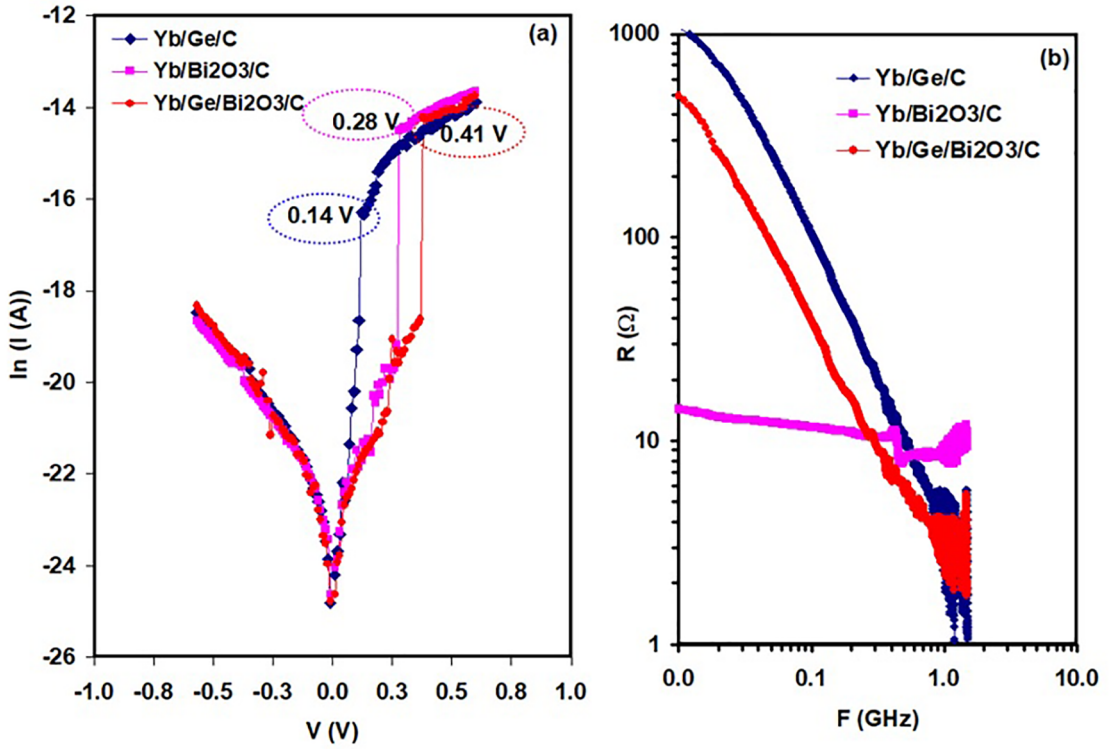
Figure 3. (a) The current-voltage characteristics and (b) the resistance spectra for the Yb/Ge/C, Yb/Bi$_2$O$_3$/C and Yb/Ge/Bi$_2$O$_3$/C channels.
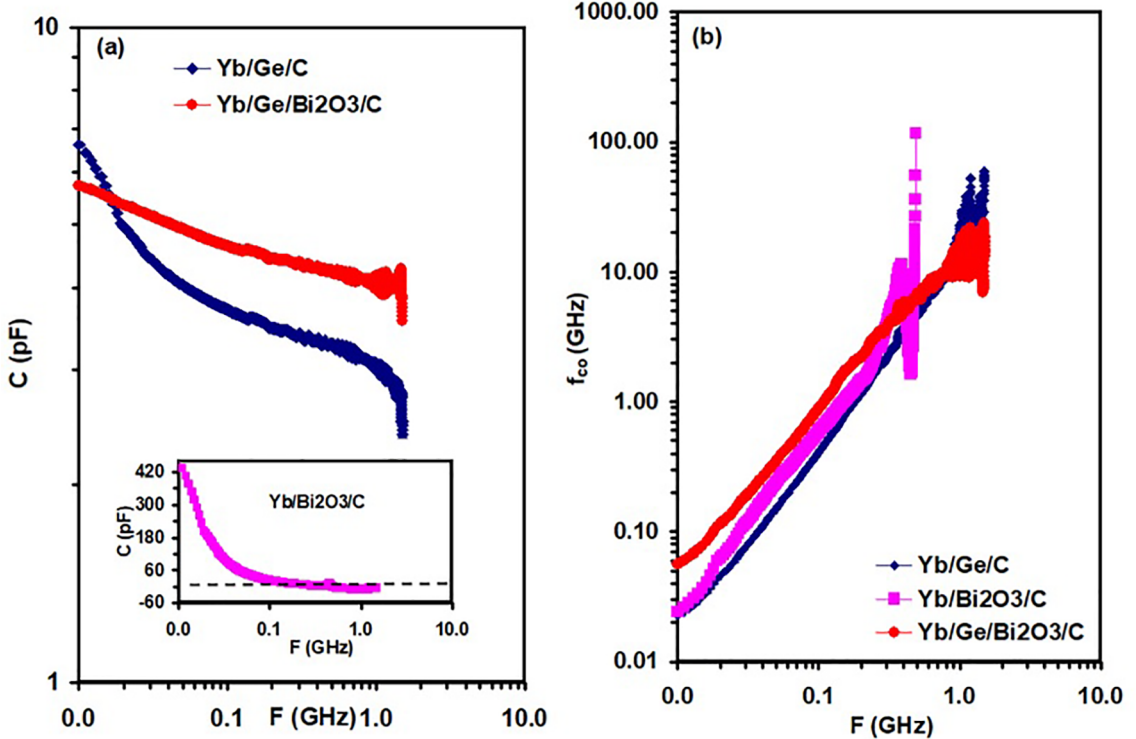

Figure 4. The capacitance and (b) the microwave cutoff frequency spectra for the Yb/Ge/C and Yb/Ge/Bi$_2$O$_3$/C channels. The inset of (a) shows the capacitance spectra for Yb/Bi$_2$O$_3$/C channel.

capacitance decreases from 460 pF to 2.2 pF as the frequency increases from 0.01 to 0.477 GHz and then exhibits negative capacitance effect reaching a value of -4.58 pF at 1.5 GHz. This feature is very interesting as it indicates the ability of the designed three terminal devices to exhibit parasitic capacitance cancelation. Such property makes the Yb/Ge/Bi_2O_3/C device attractive for use as negative capacitance field effect transistors [24,25]. Such property is very necessary to reduce noises that is associated with signal propagation [24,25]. The negative capacitance in electronic devices arises from the loss of interfaces charges, charge injection, interface states, or minority-carrier injection effects [13,26].

As a complementary information we have calculated the microwave cutoff frequency ($f_{co} = (2 \pi RC)^{-1}$). The cutoff frequency spectra for the three channels are shown in Fig. 4 (b). The figure illustrates the power dependence of the cutoff frequency on the propagating signal frequency. It increases with increasing signal frequency indicating wide range of microwave cavity control. The microwave cutoff frequency represents the frequency at which the electromagnetic energy flowing through the channel begins to be reduced (attenuated or reflected) rather than passing through. Thus, the curves which are presented in Fig. 4 (b) illustrate the possibility to design any band pass/reject filter through controlling the input signal frequency. In accordance with the figure, if the imposed signal frequency is fixed at 1.5 GHz, electromagnetic waves can pass through the first, second and third channel of the device till a cutoff frequency of value of 60, 22 and 116 GHz is, respectively, reached. It indicates high ability of data transfer when the device under study is used as band pass/reject filters [27,28].

4. Conclusions

In the current study, we have explored the physical properties and demonstrated some possible applications of the Ge/Bi_2O_3 interfaces. While the high rate of evaporation forced the formation of monoclinic Bi_2O_3 on the cubic Ge film, the current voltage characteristics revealed the "on/off" switching property. The device also appeared as promising electronic circuit elements suitable for negative capacitance production, noise reduction and for high rates of data transfer through the device channels. The novelty of this structure mostly relates to the frequency control of the resistance, capacitance and microwave cutoff frequency.

5. Acknowledgements

6. References

1. Wang K, Wu H, Meng Y, Zhang Y, Wei Z. Integrated energy storage and electrochromic function in one flexible device: an energy storage smart window. *Energy & Environmental Science*. 2012;5(8):8384-8389.

2. Somani PR. Pressure sensitive multifunctional solar cells using carbon nanotubes. *Applied Physics Letters*. 2010;96(17):173504.

3. Najim AA, Muhi MA, Gbashi KR, Salih AT. Synthesis of Efficient and Effective γ-MnO_2/a-Bi_2O_3/a-Si Solar Cell by Vacuum Thermal Evaporation Technique. *Plasmonics*. 2017;13(3):891-895.

4. Banerjee S, Chakravorty D. Multifunctional Mesoporous Nanocomposites. *Materials Science Forum*. 2013;736:98-119. DOI: doi.org/10.4028/www.scientific.net/MSF.736.98

5. Chang M, Hu H, Zhang Y, Chen D, Wu L, Li X. Improving Visible Light-Absorptivity and Photoelectric Conversion Efficiency of a TiO_2 Nanotube Anode Film by Sensitization with Bi_2O_3 Nanoparticles. *Nanomaterials*. 2017;7(5):104.

6. Lattyak C, Ravekes RE, Steenhoff V, Vehse M, Agert C. Ultrathin Resonant-Cavity-Enhanced Amorphous Germanium Solar Cells on ZnO Honeycomb Electrodes. *IEEE Journal of Photovoltaics*. 2017;8(1):3-7.

7. Jia L, Fan G, Zi W, Ren X, Liu X, Liu B, et al. Ge quantum dot enhanced hydrogenated amorphous silicon germanium solar cells on flexible stainless steel substrate. *Solar Energy*. 2017;144:635-642. DOI: doi.org/10.1016/j.solener.2017.01.042

8. Si FT, Olindo I, Zeman M. Thin-film amorphous silicon germanium solar cells with p- and n-type hydrogenated silicon oxide layers. *Solar Energy Materials and Solar Cells*. 2017;163:9-14. DOI: doi.org/10.1016/j.solmat.2017.01.001

9. Kim Y, Kim K, Kim CZ, Jung SH, Kang HK, Park WK, et al. Highly efficient epitaxial Ge solar cells grown on GaAs (001) substrates by MOCVD using isobutylgermane. *Solar Energy Materials and Solar Cells*. 2017;166:127-131. DOI: doi.org/10.1016/j.solmat.2017.03.015

10. Zhao X, Li D, Zhang T, Conrad B, Wang L, Soeriyadi AH, et al. Short circuit current and efficiency improvement of SiGe solar cell in a GaAsP-SiGe dual junction solar cell on a Si substrate. *Solar Energy Materials and Solar Cells*. 2017;159:86-93. DOI: doi.org/10.1016/j.solmat.2016.08.037

11. Muliuk G, Ye N, Zhang J, Abbasi A, Trindade A, Bower C, et al. *Transfer print integration of 40 Gbps germanium photodiodes onto silicon photonic ICs*. In: 43rd European Conference on Optical Communication (ECOC 2017); 2017 Sep 17-21; Gothenburg, Sweden. DOI: 10.1109/ECOC.2017.8346097

12. Salamin Y, Ma P, Emboras A, Fedoryshyn Y, Cheng B, Hafner C, et al. *High Speed Photoconductive Plasmonic Germanium Detector*. In: CLEO: Science and Innovations 2017; 2017 May 14-19; San Jose, CA, USA. Paper STu1N-2. DOI: doi. org/10.1364/CLEO_SI.2017.STu1N.2

13. Khusayfan NM, Qasrawi AF, Khanfar HK. Impact of Yb, In, Ag and Au thin film substrates on the crystalline nature, Schottky barrier formation and microwave trapping properties of Bi$_2$O$_3$ films. *Materials Science in Semiconductor Processing*. 2017;64:63-70. DOI: doi.org/10.1016/j.mssp.2017.02.028

14. Najim AA. Synthesis and characterizations of (δ-Bi$_2$O$_3$)$_{0.93}$(TiO$_2$)$_{0.07}$ thin films grown by PLD technique for optoelectronics. *Materials Science in Semiconductor Processing*. 2017;71:378-381. DOI: doi.org/10.1016/j.mssp.2017.08.035

15. Abu-Dief AM, Mohamed WS. α-Bi$_2$O$_3$ nanorods: synthesis, characterization and UV-photocatalytic activity. *Materials Research Express*. 2017;4(3):035039. DOI: doi.org/10.1088/2053-1591/aa6712

16. Sindhu S, Jabeen Fatima MJ, Niveditha CV. α-Bi$_2$O$_3$ photoanode in DSSC and study of the electrode-electrolyte interface. *RSC Advances*. 2015;5(95):78299-78305. DOI: 10.1039/C5RA12760B

17. Malligavathy M, Iyyapushpam S, Nishanthi ST, Padiyan DP. Remarkable catalytic activity of Bi$_2$O$_3$/TiO$_2$ nanocomposites prepared by hydrothermal method for the degradation of methyl orange. *Journal of Nanoparticle Research*. 2017;19(4):144. DOI: 10.1007/s11051-017-3806-x

18. Sze SM, Ng KK. *Physics of Semiconductor Devices*. Hoboken: John Wiley & Sons; 2006.

19. Tsu R, Fiddy MA, Her T. High mobility and high concentration Type-III heterojunction FET. *AIP Conference Proceedings*. 2018;1934(1):020002.

20. Madelung O. *Semiconductors: Data Handbook*. Berlin Heidelberg: Springer Verlag; 2012.

21. Bandyopadhyay S, Dutta S, Dutta A, Pradhan SK. Mechanosynthesis of Nanocrystalline Fully Stabilized Bcc γ-phase of Bi$_2$O$_3$ without Any Additive: Manifestation of Ferroelasticity in Microstructure, Optical and Transport Properties. *Crystal Growth & Design*. 2018;18(11):6564-6572. DOI: 10.1021/acs.cgd.8b00768

22. Ge J, Koirala P, Grice CR, Roland PJ, Yu Y, Tan X, et al. Oxygenated CdS Buffer Layers Enabling High Open-Circuit Voltages in Earth-Abundant Cu$_2$BaSnS$_4$ Thin-Film Solar Cells. *Advanced Energy Materials*. 2017;7(6):1601803.

23. Khusayfan NM, Khanfar HK. Impact of Mg layer thickness on the performance of the Mg/Bi$_2$O$_3$ plasmonic interfaces. *Thin Solid Films*. 2018;651:71-76. DOI: doi.org/10.1016/j.tsf.2018.02.025

24. Jiang C, Si M, Liang R, Xu J, Peide DY, Alam MA. A Closed Form Analytical Model of Back-Gated 2-D Semiconductor Negative Capacitance Field Effect Transistors. *IEEE Journal of the Electron Devices Society*. 2018;6:189-194.

25. Alghamdi S, Si M, Yang L, Peide DY. *Low frequency noise in MOS 2 negative capacitance field-effect transistor*. In: 2018 IEEE International Reliability Physics Symposium (IRPS); 2018 Mar 11-15; Burlingame, CA, USA.

26. Al-Hazmi F, Yakuphanoglu F. Cu$_2$ZnSnS$_4$: graphene oxide nanocomposites based photoresponse devices. *Journal of Alloys and Compounds*. 2015;653:561-569. DOI: doi.org/10.1016/j.jallcom.2015.08.238

27. Han SJ, Garcia AV, Oida S, Jenkins KA, Haensch W. Graphene radio frequency receiver integrated circuit. *Nature Communications*. 2014;5:3086. DOI: doi.org/10.1038/ncomms4086

28. Curtis J, Pham AV, Aryanfar F. Ka-band doherty power amplifier with 26.9 dBm output power, 42% peak PAE and 32% back-off PAE using GaAs PHEMTS. *IET Microwaves, Antennas & Propagation*. 2016;10(10):1101-1105. DOI: 10.1049/iet-map.2015.0818